

Detection of unidentified infrared bands in a $H\alpha$ filament in the dwarf galaxy NGC1569 with AKARI

Takashi Onaka¹, Hiroko Matsumoto^{1,*}, Itsuki Sakon¹, and Hidehiro Kaneda²

¹ Department of Astronomy, Graduate School of Science, The University of Tokyo, Bunkyo-ku, Tokyo 113-0033, Japan
e-mail: onaka@astron.s.u-tokyo.ac.jp; isakon@astron.s.u-tokyo.ac.jp

² Graduate School of Science, Nagoya University Chikusa-ku, Nagoya 464-8602, Japan
e-mail: kaneda@u.phys.nagoya-u.ac.jp

ABSTRACT

Context. We report the detection of unidentified infrared (UIR) bands in a filamentary structure associated with $H\alpha$ emission in the starburst dwarf galaxy NGC1569 based on imaging and spectroscopic observations of the *AKARI* satellite.

Aims. We investigate the processing and destruction of the UIR band carriers in an outflow from NGC1569.

Methods. We performed observations of NGC1569 for 6 infrared bands (3.2, 4.1, 7, 11, 15, and 24 μm) with the Infrared Camera (IRC) onboard *AKARI*. Near- to mid-infrared (2–13 μm) spectroscopy of a $H\alpha$ filament was also carried out with the IRC.

Results. The extended structure associated with a $H\alpha$ filament appears bright at 7 μm . Since the IRC 7 μm band (S7) efficiently traces the 6.2 and 7.7 μm UIR band emission, the IRC imaging observations suggest that the filament is bright at the UIR band emission. Follow-up spectroscopic observations with the IRC confirm the presence of 6.2, 7.7, and 11.3 μm emission in the filament. The filament spectrum exhibits strong 11.3 μm UIR band emission relative to the 7.7 μm band compared to the galaxy disk observed with the Infrared Spectrograph on *Spitzer*. The near-infrared spectrum also suggests the presence of excess continuum emission in 2.5–5 μm in the filament.

Conclusions. The presence of the UIR bands associated with a $H\alpha$ filament is found by *AKARI*/IRC observations. The $H\alpha$ filament is thought to have been formed by the galactic outflow originating from the star-formation activity in the disk of NGC1569. The destruction timescale of the UIR band carriers in the outflow is estimated to be much shorter ($\sim 1.3 \times 10^3$ yr) than the timescale of the outflow (~ 5.3 Myr). Thus it is unlikely that the band carriers survive the outflow environment. Alternatively, we suggest that the band carriers in the filaments may be produced by the fragmentation of large carbonaceous grains in shocks, which produces the $H\alpha$ emission. The NIR excess continuum emission cannot be accounted for by free-free emission alone and a hot dust contribution may be needed, although the free-free emission intensity estimated from $H\text{I}$ recombination lines has a large uncertainty.

Key words. Galaxies: ISM – Infrared: galaxies – dust, extinction – Galaxies: individual: NGC1569

1. Introduction

From the near-infrared (NIR) to mid-infrared (MIR) region, a set of prominent emission features at 3.3, 3.4, 6.2, 7.7, 8.6, and 11.3 μm are detected for the various celestial objects. Faint companion bands are also present in the 5–13 μm spectral range. They are often called the unidentified infrared (UIR) bands because of the difficulty in identifying the band carriers at an early epoch of their discovery. Space observations have added the 17 μm feature complex to the UIR band family (van Kerckhoven et al. 2000; Werner et al. 2004). The UIR bands have been observed in $H\text{II}$ regions, reflection nebulae, post-asymptotic giant branch (AGB) stars, and planetary nebulae (PNe) (e.g., Peeters et al. 2002). They are also ubiquitously seen in the diffuse Galactic radiation (Giard et al. 1988; Onaka et al. 1996; Mattila et al. 1996; Tanaka et al. 1996; Onaka 2004) as well as in external galaxies (Helou et al. 2000; Lu et al. 2003; J. D. Smith et al. 2007), suggesting that the band carriers belong to major constituents of the interstellar matter (e.g., Draine et al. 2007). Since their intensity is found to be well correlated with the far-infrared (FIR) intensity and can thus be used as a useful measure of the star-formation activity (Onaka 2000; Peeters et al. 2004), and they are prominent features in the MIR that can be detected even in distant galaxies (e.g., Lutz et al.

2005), the understanding of the properties as well as the formation and destruction processes in the interstellar space of the band carriers is significant not only to the study of the interstellar medium (ISM), but also to the study of physical conditions and star-formation activities in the remote universe.

While it is generally thought that the UIR bands originate in emitters or emitting atomic groups containing polycyclic aromatic hydrocarbons (PAHs) or PAH-like atomic groups of carbonaceous materials (Léger & Puget 1984; Allamandola et al. 1985; Sakata et al. 1984; Papoular et al. 1989), the exact nature, formation, and destruction of the band carriers are not yet fully understood (see Tielens 2008, for a recent review). Carbon-rich AGB stars are thought to be one of the major sources of the band carriers (Frenklach & Feigelson 1989; Latter 1991; Cherchneff et al. 1992; Galliano et al. 2008a). The carriers may also be formed by the fragmentation of large carbonaceous grains (Omont 1986; Jones et al. 1996; Greenberg et al. 2000) or in situ within dense clouds (Herbst 1991). On the other hand, the carriers can be destroyed efficiently by interstellar shocks (Jones et al. 1996) and within ionized gas (e.g., Matsumoto et al. 2008, references therein). Few observational studies have, however, so far been carried out for the life cycle of the band carriers in the ISM.

Peeters et al. (2002) show that there are at least three distinct classes of UIR-band objects present as far as the peak

* Present address: Nikkei Inc. Chiyoda-ku, Tokyo 100-8066, Japan

wavelengths of the 6.2, 7.7, and 8.6 μm MIR UIR bands are concerned. Class A objects, to which H II regions and isolated Herbig Ae/Be stars belong, show the band peaks at short wavelengths relative to Class B objects, which include PNe and post-AGB stars. Class C objects exhibit quite different spectra compared to class A and B objects. The variation in the peak wavelengths suggests possible processing of the band carriers in the ISM. The origin of the difference between class A and B objects may be attributed to the inclusion of hetero atoms (Peeters et al. 2002) or carbon isotopes in the band carriers (Wada et al. 2003). On the other hand, the UIR band spectrum observed in the diffuse Galactic radiation does not exhibit any systematic variations in the inner part of the Galaxy (Chan et al. 2001; Kahanpää et al. 2003), whereas Sakon et al. (2004) detected small variations in the band ratio and the peak wavelength between the inner part of the Galaxy and the outer part. Variations in the band spectra of external galaxies and within a given galaxy are also generally small (e.g., J. D. Smith et al. 2007; Gordon et al. 2008). Studies, however, indicate that elliptical galaxies show UIR band spectra very different from those in spiral galaxies, where the usually strong MIR UIR bands (6.2, 7.7, and 8.6 μm) are weak or absent, but the 11.3 μm band is clearly present (Kaneda et al. 2005). The 3.3 μm band seems also to be absent in the elliptical galaxy NGC1316, which exhibits the 11.3 μm band (Kaneda et al. 2007). The weak MIR UIR bands relative to that at 11.3 μm are also seen in galaxies that harbor a low-luminosity active galactic nucleus (AGN, J. D. Smith et al. 2007), some of which are also elliptical galaxies. Smaller scale variations in the same sense have also been detected in the interarm region of NGC6946 (Sakon et al. 2007) and halo regions of galaxies (Irwin & Madden 2006; Galliano et al. 2008b), suggesting that a common mechanism changes the band ratio (Onaka et al. 2008). Weak MIR UIR bands may be seen in tenuous plasma environments. Processing of the band carriers in these environments may be responsible for the variation.

The UIR bands in low-metallicity dwarf galaxies are important to study because their characteristics may represent very young galaxies and the band carriers may not be fully developed in these environments if carbon-rich AGB stars are the main source of the carriers (Galliano et al. 2008b). The UIR bands are very weak or almost absent in dwarf galaxies that have metallicities $\log[\text{O}/\text{H}]+12 \lesssim 8.1$ (Engelbracht et al. 2008). Since these low-metallicity dwarf galaxies are also known to be associated with high star-formation activities, the deficiency in the UIR bands in low metallicity environments can be attributed to low carrier formation efficiency at low metallicity, rapid destruction of the band carriers by strong radiation fields (Wu et al. 2006, 2007), frequent supernova shock passages that destroy the carriers (O’Halloran et al. 2006), or deficiency in carbon-rich AGB stars that produce the carriers in young galaxies (Galliano et al. 2008b).

In this paper, we report the results of infrared imaging and spectroscopic observations of the low-metallicity dwarf galaxy NGC1569 with the Infrared Camera (IRC) onboard *AKARI* (Murakami et al. 2007; Onaka et al. 2007b). NGC1569 is a nearby starburst dwarf galaxy of metallicity of about a quarter of solar, i.e., its values of $12 + \log(\text{O}/\text{H})$ range from 8.19 to 8.37 (Greggio et al. 1998, references therein). *Hubble Space Telescope* observations indicate that it is located in the IC 342 group of galaxies at a distance of 3.36 ± 0.20 Mpc (Grocholski et al. 2008). Several filamentary structures that extend out to 1 kpc have been detected in H α (Hunter et al. 1993; Heckman et al. 1995; Martin 1998; Westmoquette et al. 2007a,b, 2008). Associated X-ray emission has also been de-

tected, suggesting that these filaments are formed by the galactic outflow (Martin et al. 2002). NGC1569 has two well-known super-star clusters (SSCs) and numerous compact clusters (Hunter et al. 2000). Some remain deeply embedded in dense clouds (Tokura et al. 2006). NGC1569 has probably experienced three major epochs of star formation over the entire galaxy that peaked at 5–27, 32–100, and ≥ 2000 Myr ago (Greggio et al. 1998; Angeretti et al. 2005; Grocholski et al. 2008). Shock-ionized gas appears to be detected (Buckalew et al. 2000; Buckalew & Kobulnicky 2006), which is indicative of recent star-formation activity (Westmoquette et al. 2007b). The H I inflow stream may have interacted with the galaxy disk in the region of a velocity-crowding ‘hot spot’ and triggered the star formation (Stil & Israel 1998; Mühle et al. 2005).

The metallicity of NGC1569 is slightly above the threshold for the presence of UIR bands. ISOCAM observations of NGC1569 show that the entire galaxy disk is dominated by UIR band emission (Madden et al. 2006), although it is weak or absent locally around SSCs and H II regions (Tokura et al. 2006). To investigate the distribution and possible spatial variations in the UIR bands in NGC1569, imaging and spectroscopic observations were executed with *AKARI* as part of the mission program ‘‘ISM in our Galaxy and Nearby Galaxies’’ (ISMGN; Kaneda et al. 2009a). The observations and the data reduction are described in Sect. 2 and the results are presented in Sect. 3. The origin of the UIR band carriers is discussed in Sect. 4. A summary is given in Sect. 5.

2. Observations and data reduction

IRC imaging observations of NGC1569 were carried out on 2006 September 9 in the two-filter mode (AOT: IRC02, Onaka et al. 2007b). The size of the galaxy is a few arcminutes. Owing to the wide field-of-view of the IRC ($\sim 10' \times 10'$), one pointing observation covers the entire galaxy. With two pointing observations, we obtained images in the 6 bands N3 (3.2 μm), N4 (4.1 μm), S7 (7.0 μm), S11 (11.0 μm), L15 (15.0 μm), and L24 (24.0 μm) because the NIR (N3 and N4) and the MIR-S (S7 and S11) channels share the field-of-view and observe the same area of sky at the same time. The MIR-L (L15 and L24) observes a sky about 20' from the NIR/MIR-S.

Spectroscopic observations were carried out with AOT IRC04 with the NIR and MIR-S slit mode (Ns), whose width is 5'' and length is about 1', for 1.8–13.4 μm . The center of the slit was placed at the position of a H α filament, where the presence of the UIR bands was inferred from the imaging observations (see Table 2 and Fig. 2b). The spectrum consists of 3 segments. The spectrum of 1.8–5.5 μm was taken with the prism (NP) in the NIR channel, while the spectra of 4.6–9.2 μm and 7.2–13.4 μm were taken with two gratings, SG1 and SG2, in the MIR-S, respectively. Table 1 summarizes the observation log.

The imaging data were processed with the IRC imaging toolkit version 20071017, which includes linearity correction, dark current subtraction, flat-fielding, correction for the image distortion, and coaddition of dithered images. The toolkit algorithm produces final images with the pixel field-of-view of 1'446 for N3 and N4, 2'340 for S7 and S11, and 2'384 for L15 and L24. The images produced by the toolkit were processed by our own software. The original images are in the array coordinates. An area of 5'5 \times 5'0 is extracted in the equatorial coordinates and then smoothed with a Gaussian of FWHM 3'5 for the N3 and N4 images and 7'' for the other 4 bands to adjust the spatial resolution with respect to each other without appreciable degradation of the image quality in each band (Onaka et al. 2007b).

Table 1. IRC observation log of NGC1569

Obs. mode	Obs. ID	Date	AOT ^a	Filter
Imaging	1400423.1	2006 September 9	IRC02 a:N	N3, N4, S7, & S11
	1400424.1	2006 September 9	IRC02 a:L	L15 & L24
Spectroscopy	1400701.1	2007 March 8	IRC04 a:Ns	prism (NP) & grisms (SG1 and SG2)

^a Astronomical Observation Template. See ASTRO-F Observer's Manual for details of the parameters (<http://www.ir.isas.jaxa.jp/ASTRO-F/Observation/ObsMan/afobsman32.pdf>).

The contribution from the stellar photospheric emission is subtracted except for the N3 image, which is used as a reference after subtracting the constant sky background. The flux ratio relative to N3 in units of ADU is estimated for the average stellar spectrum based on the fluxes of red giant stars used in the flux calibration as 0.69, 0.073, 0.050, 0.0098, and 0.0017 for N4, S7, S11, L15, and L24, respectively (Tanabé et al. 2008). The stellar flux subtraction is important only in the galactic disk region and does not make a significant effect except for the N4 image.

The flux calibration of the IRC for point sources is more accurate than 10% for all the photometric bands (Tanabé et al. 2008), though the calibration for the diffuse emission is still underway. The uncertainty of about 30% is expected for the absolute calibration for the diffuse emission because the IRC uses the same types of detector arrays as the IRAC on *Spitzer* (Reach et al. 2005; Cohen et al. 2007). Since the relative flux has a far smaller uncertainty, the following discussion focuses on the relative fluxes among the bands or colors rather than on the absolute flux values.

The spectroscopic data were processed with the IRC spectroscopy toolkit version 20090211. Each segment of the spectrum was truncated at the wavelengths where the signal-to-noise ratio becomes low: NP was truncated at 2.3 and 5.0 μm , SG1 at 5.5 and 8.2 μm , and SG2 at 8.0 and 13.2 μm . The accurate position at which the spectrum was taken was estimated for the reference image of N3 obtained during the same pointing observation. The original spectrum has contributions from NGC1569, the diffuse Galactic emission, and the zodiacal light. Since we did not perform separate observations to obtain the background spectrum, we chose a "sky" on the slit near the edge, where the contribution of NGC1569 is minimal, and subtracted the sky spectrum from the "filament" spectrum. Table 2 summarizes the center positions where the spectra of the filament and sky were extracted (see also Fig. 2b). The pixel scale was different between the NIR and MIR-S channels. The spectra were extracted for a slit length of 5 and 3 pixels (7".3 and 7".0) for the NIR and MIR-S, respectively, and averaged. We note that even for the SG1 and SG2 spectra the observed position was slightly different because the SG1 and SG2 grisms did not produce the same optical path. The SG1 spectra were smoothed by taking a moving average over 4 pixels in the spectral direction to increase the signal-to-noise ratio without significant degradation of the spectral resolution. The SG2 spectra were smoothed by a 3-pixel moving average. The NP spectrum of the filament longer than 4.3 μm was smoothed by taking a 2-pixel running average, while that shortward of 4.3 μm was not smoothed to prevent decreasing the spectral resolution since NP spectra have lower resolution at shorter wavelengths. These smoothing processes produced a spectral resolution ($\lambda/\Delta\lambda$) of about 30 at the central wavelength of each segment. The raw sky spectrum of NP had a low signal-to-noise ratio and was smoothed by a 5-pixel moving average in the wavelength direction based on the assumption that the sky spectrum did not have significant features.

Table 2. Positions of the spectrum extracted

Object	Center position (J2000) ^a	
	R.A.	Dec
Filament	04 ^h 30 ^m 41 ^s .1	64° 51' 03".4
Sky	04 ^h 30 ^m 39 ^s .0	64° 50' 59".8

^a The spectrum was extracted over 5" \times 7".3 and 5" \times 7".0 regions, for the NIR and MIR-S, respectively (see text).

3. Results

3.1. Imaging

Figure 1 shows IRC 6-band images of NGC1569. Uniform sky background was subtracted from all the images. The N3 and N4 images exhibit similar structures, in which stellar contributions are dominant. The appearance of the galaxy drastically changes from the S7 image. The emission in the N3 and N4 images is dominated by the stellar radiation, whereas the emission longer than the S7 arises dominantly from the interstellar matter of the galaxy. The S7 image clearly resolves two peaks seen in ISOCAM observations (Madden et al. 2006) and indicates spotty structures in the galaxy disk. The western peak is located at the slightly western side of SSC A (e.g., Hunter et al. 2000). The hot spot or the region of velocity crowding, which is seen in the H I map and suggested as the impact location of the infalling gas onto the galaxy disk (Mühle et al. 2005), is located further west of the western MIR peak. The S7 band consists of major MIR UIR band emission (6.2, 7.7, and 8.2 μm bands) and thus traces the UIR band emission efficiently (Ishihara et al. 2007). Both the 11.3 μm UIR band and continuum emission could make a significant contribution to the S11 image. The continuum emission dominates in the L15 and L24 bands, which traces regions active in star formation (e.g. Onaka et al. 2007a; Draine et al. 2007). NGC1569 contains a number of SSCs and thus the L15 and L24 bands are probably dominated by the contribution of the emission from active star-forming regions. The disk emission in S7 is dominated by the UIR emission. A filamentary structure also extends from the western edge of the galaxy disk to the south in the S7 image. This filament is also detected in the S11 image. In the L15 and L24 images, the disk emission becomes smoother, whereas the diffuse emission appears to extend to the north-east direction. A faint trace of the filamentary structure can be discerned, but it is not as clear as in the S7 and S11 images.

Figure 2a presents a three-band color image (N4, S7, and L15), which indicates that the filamentary structure is indeed bright in the S7 band (green) and there is no appreciable associated stellar component (blue). This structure corresponds to the western arm or filament 6 recognized in H α images (Hodge 1974; Hunter et al. 1993; Westmoquette et al. 2008). The associated X-ray emission strongly infers that the filament was formed by the shock of a galactic outflow originating in the SSC A re-

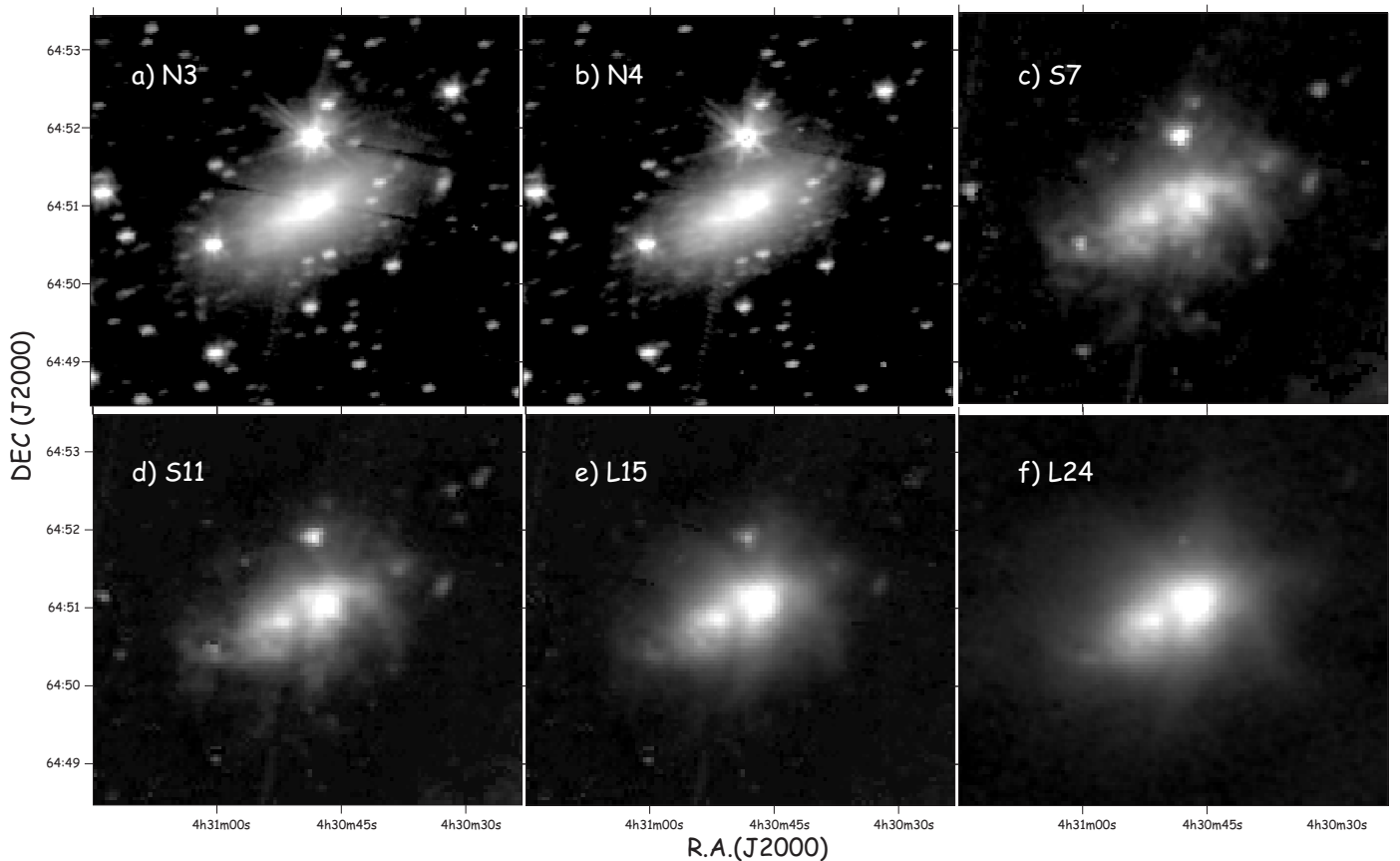


Fig. 1. AKARI/IRC 6-band images of NGC1569. The image size is $5'.5 \times 5'.0$. a) N3 ($3.2 \mu\text{m}$), b) N4 ($4.1 \mu\text{m}$), c) S7 ($7.0 \mu\text{m}$), d) S11 ($11.0 \mu\text{m}$), e) L15 ($15.0 \mu\text{m}$), and f) L24 ($24 \mu\text{m}$).

gion of the disk (Martin 1998; Martin et al. 2002; Greve et al. 2002). Figure 2b shows the S7 image superimposed on the $\text{H}\alpha$ emission in contours (Hunter & Elmegreen 2004). It shows good agreement between the S7 and $\text{H}\alpha$ emission of the filament in position and suggests that the entire S7 emission may be more extended than the $\text{H}\alpha$ emission around the galaxy. It can also be seen that the S7 emission of the filament is located at a slightly western side of the $\text{H}\alpha$ emission. Since the X-ray emission peaks at the eastern side of the $\text{H}\alpha$ filament (Martin et al. 2002), the peak of the emission is close in position to that of the X-ray, $\text{H}\alpha$, and $7 \mu\text{m}$ emission from east to west.

A similarity between the S7 and S11 images infers that the $11.3 \mu\text{m}$ band emission is also bright in the filament. The present imaging observations appear to detect both UIR bands in the $\text{H}\alpha$ filament and an extended component around NGC1569. The $\text{H}\alpha$ filament is probably formed by the outflow associated with the X-ray emission, suggesting that the UIR band emission is also enhanced by the outflow. We carried out spectroscopic observations of the filament to confirm the presence of the UIR bands.

3.2. Spectroscopy

Figure 3 shows AKARI/IRC spectra taken at the position of the $\text{H}\alpha$ filament. The NP spectroscopy clearly shows the continuum emission at the filament position over the background (Fig. 3a). It cannot be accounted for by photospheric emission from stars, which should decrease far more sharply towards longer wavelengths. The NP spectrum also exhibits the $3.3 \mu\text{m}$ UIR band. Two spiky features at 3.75 and $4.05 \mu\text{m}$ may be H I recombination lines of $\text{P}\delta$ and $\text{B}\alpha$, but the low spectral resolution of NP,

even in the unsmoothed spectrum, makes clear identification difficult. If these are H I recombination lines, there should be a $\text{P}\delta$ line at $3.3 \mu\text{m}$ that overlaps with the UIR band. Its intensity is roughly $0.7 \times \text{P}\gamma$ for the case B condition with the electron temperature of 10^4 K and density of 10^4 cm^{-3} . Thus, even if the contribution of $\text{P}\delta$ is taken into account, the presence of the $3.3 \mu\text{m}$ UIR band is secure.

The SG1 and SG2 spectra are dominated by the zodiacal emission, which steeply increases towards longer wavelengths (Figs. 3b and 3c). The level of the sky background emission is in good agreement with the estimated zodiacal light intensity from COBE observations (Kelsall et al. 1998). The sky-subtracted SG1 and SG2 spectra do not show a steep rise towards longer wavelengths, implying that star formation is not very active in the filament (Onaka et al. 2007a). The sky spectra also appear to contain UIR bands, which can be attributed partly to the foreground Galactic emission. There may also be a contribution from the emission of NGC1569 (see Fig. 2b). Thus the sky-subtracted filament spectra may underestimate the emission from the filament. According to the investigation by Sakon et al. (2004), the contribution of the Galactic emission to the UIR bands is estimated approximately from the FIR intensity about the position of NGC1569. The contribution to the observed UIR band emission is estimated to be about 30–70% from the FIR intensity of 40 and 70 MJy sr^{-1} at 100 and $140 \mu\text{m}$, respectively. This number is compatible with the UIR band emission in the sky spectrum. The background-subtracted spectra clearly exhibits the UIR bands at 6.2 , 7.7 , and $11.3 \mu\text{m}$ in the filament, confirming that the structures seen in the S7 and S11 images are

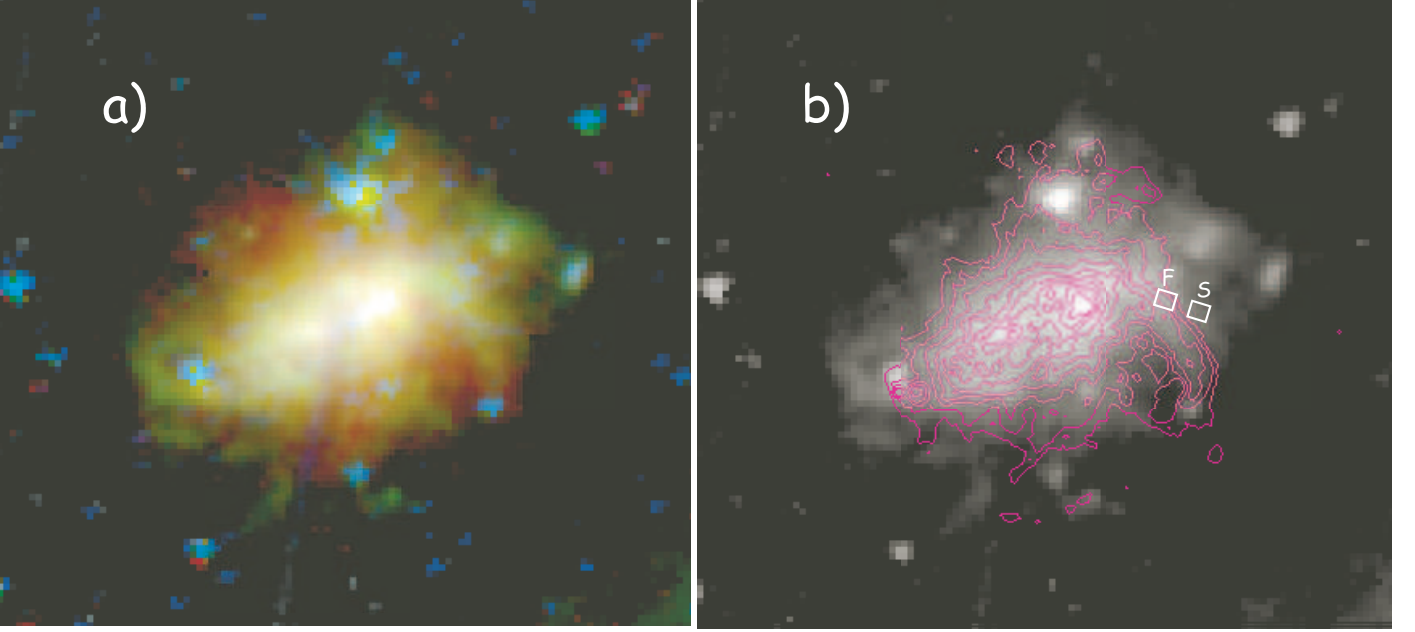


Fig. 2. a) Artificial 3-color image of NGC1569. The N4 in blue, S7 in green, and L15 in red. b) S7 image of NGC1569 superimposed with contours in a logarithmic scale of the $H\alpha$ emission (Hunter & Elmegreen 2004). The $H\alpha$ image (Hunter & Elmegreen 2004) was taken from the NASA/IPAC Extragalactic Database (NED). The white boxes indicate the positions where the filament (F) and sky (S) spectra were extracted (see text).

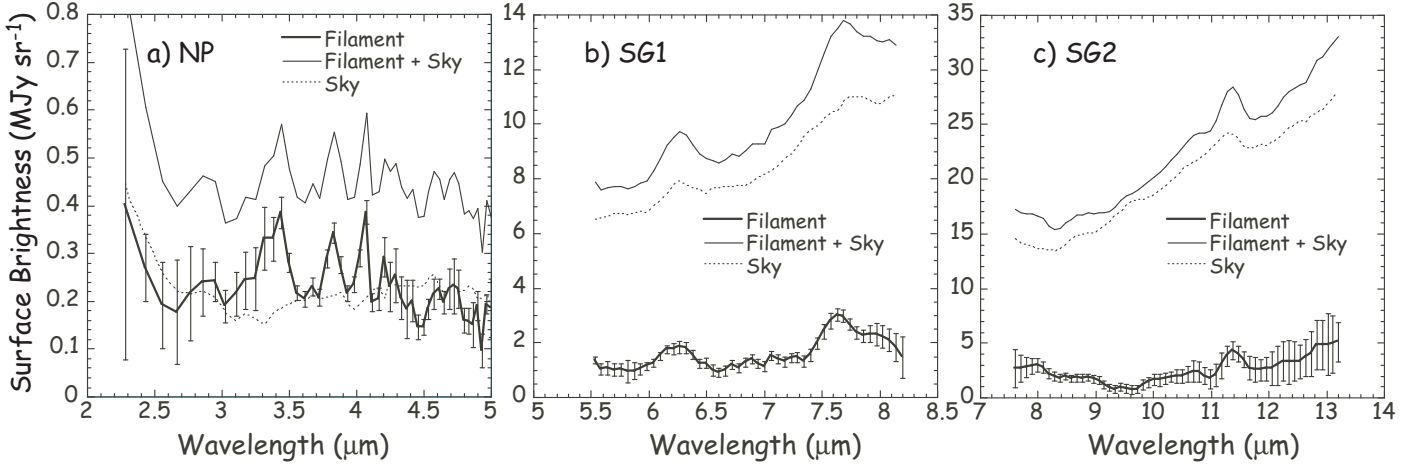


Fig. 3. AKARI/IRC spectra of the $H\alpha$ filament of NGC1569: a) NP, b) SG1, and c) SG2. The thin solid lines indicate spectra at the filament position before subtraction of the sky background and the thin dotted lines show sky spectra. The thick solid lines indicate filament spectra from which the sky spectra have been subtracted. The error bars are indicated only in the subtracted spectra to avoid confusion.

dominated by the UIR band emission. The $8.6\mu\text{m}$ UIR band is faint and is not detected by the present spectra.

4. Discussion

4.1. UIR bands in the filament

The present observations detect the UIR bands associated with a $H\alpha$ filament in NGC1569. Both FIR and UIR band emission has been detected in outflows or halo regions of several galaxies. Very extended UIR band emission has been detected in the outflow from M82 (Engelbracht et al. 2006; Kaneda et al. 2010). The $3.3\mu\text{m}$ UIR band emission associated with the outflow has been detected in NGC253 (Tacconi-Garman et al. 2005), in which emission further away from the galaxy has been de-

tected in the FIR (Kaneda et al. 2009b). The UIR band emission from the galactic halo has also been detected for several galaxies based on ISOCAM observations (Irwin & Madden 2006; Irwin et al. 2007; Galliano et al. 2008b), which indicates that the band ratio of either 6.2 or $7.7\mu\text{m}$ to the $11.3\mu\text{m}$ band emission becomes lower in the halo than in the disk region.

To investigate the UIR band ratio in the filament of NGC1569, the spectrum is fitted with a combination of a continuum emission and Lorentzians given by

$$F_\nu(\lambda) = \sum_{i=0}^n a_i \lambda^i + \sum_{i=1}^m \frac{h_i}{1 + (\lambda_i/\Delta\lambda_i)^2 (1/\lambda - 1/\lambda_i)^2}, \quad (1)$$

where λ indicates the wavelength, and the first and second terms approximate the continuum and the UIR band emission, respec-

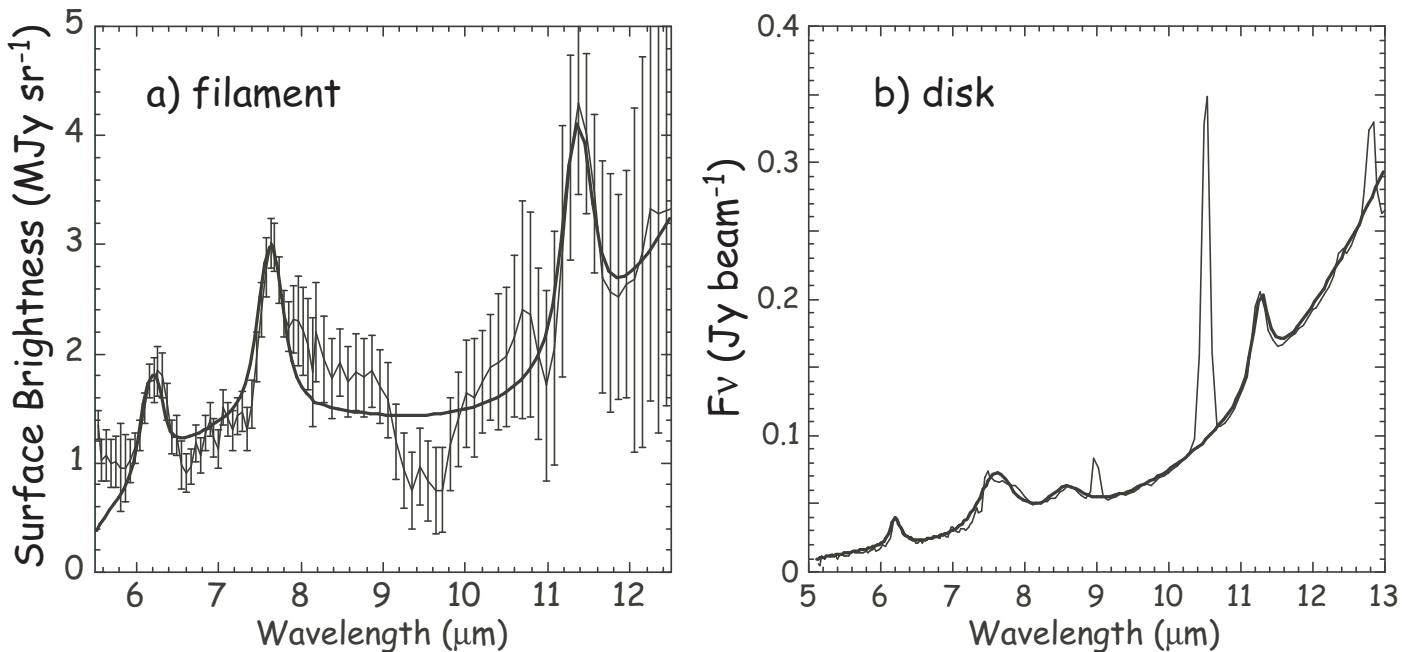


Fig. 4. a) IRC spectrum of the filament of NGC1569 (thin line) and the fitted line (thick line). b) IRS spectrum of the disk of NGC1569 (thin line) and the fitted line (thick line). Sharp lines not fitted are ionic forbidden lines ([Ar III] $9.0\ \mu\text{m}$, [S IV] $10.5\ \mu\text{m}$, and [Ne II] $12.8\ \mu\text{m}$).

tively. The parameters n and m are set to be 3: only three UIR bands (6.2 , 7.7 , and $11.3\ \mu\text{m}$) are taken into account in the fit since the $8.6\ \mu\text{m}$ is weak and its parameters cannot be constrained well by the fit. The parameters λ_i , $\Delta\lambda_i$, and h_i represent the central wavelength, width, and strength of each band component. The fitted curve is shown in Fig. 4a together with the observed spectrum. Equation (1) provides a fairly close fit except for a slight underestimate around $8\text{--}9\ \mu\text{m}$ and an overestimate in $9\text{--}10\ \mu\text{m}$. The former could be attributed to the neglect of the $8.6\ \mu\text{m}$ band. A longer wavelength component of the $7.7\ \mu\text{m}$ band may also be a contributor (see below). The latter may be possibly attributed silicate absorption.

The band strength S_i is calculated by integrating the Lorentzian in the wavenumber space and is given by

$$S_i = \pi h_i \Delta\lambda / \lambda_i^2. \quad (2)$$

Table 3 summarizes the band strength relative to the $11.3\ \mu\text{m}$ band.

Table 3. UIR band strength ratio relative to the $11.3\ \mu\text{m}$ band

Band	Filament	Disk
$6.2\ \mu\text{m}$	0.94 ± 0.29	0.71 ± 0.08
$7.7\ \mu\text{m}$	1.45 ± 0.31	3.54 ± 0.21
$8.6\ \mu\text{m}$... ^a	1.37 ± 0.13

^a The $8.6\ \mu\text{m}$ band is not included in the fit.

To compare with the UIR bands in the disk, spectra of the NGC1569 disk taken with the Infrared Spectrograph (IRS) on *Spitzer* in the low resolution modules were retrieved from the archival database (AOR key 9001984; Tajiri et al. 2008). The IRS spectra taken at the position near SSC A (R.A.: $04^{\text{h}}\ 30^{\text{m}}\ 48^{\text{s}}.17$ Dec: $+64^{\circ}\ 50'\ 54''.2$) were extracted. The IRS spectrum is

fit with Eq. (1) in the same manner as the filament spectrum except that the $8.6\ \mu\text{m}$ band is included. The IRS spectrum and the fitted spectrum are also shown in Fig. 4 and the relative band ratios are summarized in Table 3. The relative strength of the $6.2\ \mu\text{m}$ band in the filament seems to be slightly greater than in the disk. However, the $6.2\ \mu\text{m}$ band strength of the filament has a large uncertainty and it is difficult to draw conclusions about the comparison with the disk spectrum. The relative strength of the $7.7\ \mu\text{m}$ band is clearly weaker in the filament than in the galaxy disk. This is the same trend as derived from photometric measurements of halo regions of other galaxies (Irwin & Madden 2006; Galliano et al. 2008b). The 7.7 to $11.3\ \mu\text{m}$ band ratio of the IRS spectrum is in the range of values measured for normal and starburst galaxies, while the ratio for the filament is similar to those of galaxies with weak AGNs or elliptical galaxies (J. D. Smith et al. 2007; Onaka et al. 2008).

An additional inspection suggests that the weak strength of the $7.7\ \mu\text{m}$ band in the NGC1569 filament may be attributed to its narrow band width relative to those in the disk spectrum ($\Delta\lambda = 0.13 \pm 0.04\ \mu\text{m}$ to $0.31 \pm 0.02\ \mu\text{m}$). The narrow width is also suggested in Fig. 4. The $7.7\ \mu\text{m}$ UIR band is known to consist of more than two components (Peeters et al. 2002). The filament spectrum suggests that the longer wavelength component of the $7.7\ \mu\text{m}$ band may be weak or absent. There may be excess above the fitted curve around $7.8\text{--}7.9\ \mu\text{m}$, which is not included in the band strength estimate. This excess increases the band strength only within its uncertainty and does not change our conclusion that the total strength of the $7.7\ \mu\text{m}$ band is weak in the filament. The present observation suggests that the low band strength of the $7.7\ \mu\text{m}$ band in the filament may be attributed to a change in one of the components.

A low ratio of the 7.7 to $11.3\ \mu\text{m}$ band is also suggested in the outer region of our Galaxy (Sakon et al. 2004) as well as in the interarm region of NGC6946 (Sakon et al. 2007). Elliptical galaxies are an extreme case for which the 6.2 and $7.7\ \mu\text{m}$ bands are almost absent (Kaneda et al. 2005, 2008).

Kaneda et al. (2008) attributed the abnormal UIR band strengths in elliptical galaxies to the dominance of neutral PAHs. The weak 6.2 and 7.7 μm bands relative to the 11.3 μm band tend to be seen in tenuous regions and may have a common cause or be the result of processing of the band carriers in these environments (e.g., Onaka et al. 2008).

Kaneda et al. (2009b) suggest that the FIR emission detected at 6–9 kpc from the galaxy disk of NGC253 may come from the emission of outflowing dust entrained by superwinds. The UIR band carriers in the filament of NGC1569 may also be entrained by the outflow of NGC1569, which formed the H α filament. The velocity of the filament is derived to be about 90 km s⁻¹ (Westmoquette et al. 2008). If the filament were produced by the outflow produced by the star-formation activity of SSC A, the distance of 490 pc from SSC A to the position of the IRC spectrum would infer an expansion timescale of about 5.3 Myr. Observations with *Chandra* suggest that the electron temperature and density of the bubble are 3.51×10^6 K and 0.035 cm⁻³, respectively (Ott et al. 2005). Jones et al. (1996) show that thermal sputtering efficiently destroys dust grains in fast shocks (≤ 200 km s⁻¹) and that the thermal sputtering yield depends on the electron temperature and density, which can be applied even to very small grains. Using the equation given by Tielens et al. (1994), the thermal sputtering timescale for grains of 1 nm in the bubble of NGC1569 is found to be 1.3×10^3 yr, which is much shorter than the expansion timescale of the filament. Thus it seems unlikely that the band carriers in the filament originate in the galaxy disk and are entrained by the outflow without destruction. It is also unlikely that AGB stars produce a large amount of the band carriers since there appears to be neither appreciable stellar components nor strong star-forming activities in the filament. An alternative possibility for the origin of the carriers may be the fragmentation from large carbonaceous grains in shocks that produce H α emission (Jones et al. 1996). The presence of the 3.3 μm band suggests that the smallest band carriers exist in the filament, which may be consistent with the fragmentation origin. UIR band carriers formed from fragmentation may have different properties from those in the galactic disk and exhibit the weaker 7.7 μm band.

4.2. NIR excess continuum

The present observations indicate the presence of excess continuum emission in the NIR (2.5–5 μm) in the filament. NIR excess continuum emission was first reported in reflection nebulae (Sellgren et al. 1983) and then found in normal galaxies (Lu et al. 2003). It is also seen in the diffuse Galactic emission (Flagey et al. 2006). Sellgren (1984) suggests that the excess emission in reflection nebulae may be attributed to stochastically heated 3-dimensional grains consisting of 45–100 carbon atoms. The continuum emission is also found to have a distinct spatial distribution from the 3.3 μm UIR band emission (An & Sellgren 2003).

Redder colors in the NIR have been measured for irregular/Sm galaxies than for spirals (Pahre et al. 2004; Engelbracht et al. 2005; B. J. Smith et al. 2007). They have been attributed to younger stars (Pahre et al. 2004), hot dust (Engelbracht et al. 2005; Hunter et al. 2006), nebular emission, or to the 3.3 μm UIR band emission. Smith & Hancock (2009) investigate the origin of excess emission at 4.5 μm in dwarf galaxies in detail. They discuss the possibilities of a contribution from Br α , the reddening of starlight, and a nebular continuum as the origin of the excess, concluding that a combination of these three may account for the 4.5 μm excess and no significant

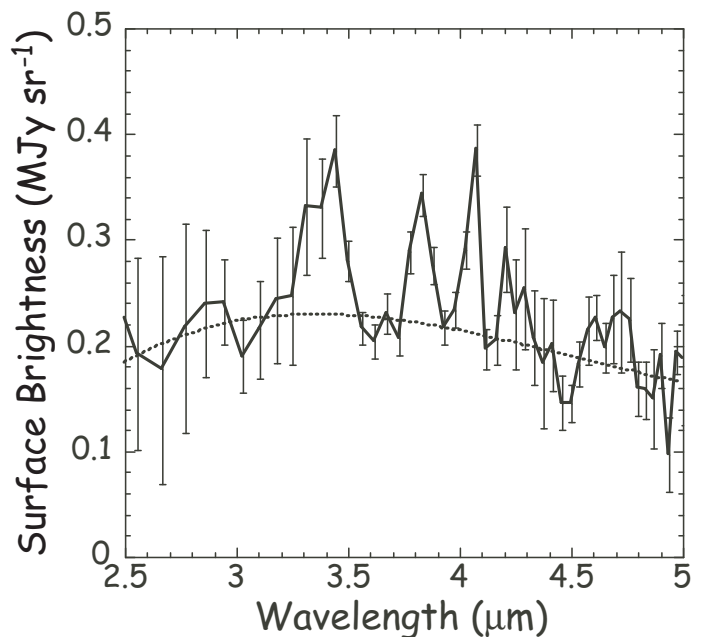


Fig. 5. NP spectrum of the filament (solid line) together with the fitted modified black body (dotted line). The fitted curve is a black body of $T = 868$ K with the emissivity of $\propto \lambda^{-2}$.

contribution of hot dust is necessary, although hot dust emission cannot be completely excluded.

The NP spectrum clearly shows the presence of excess continuum emission in addition to the 3.3 μm UIR band and line emission, if any. The continuum spectrum is rather flat in the NIR spectral range and is distinct from stellar photospheric emission. Lu et al. (2003) suggest that the excess emission seen in normal galaxies is well fitted with a modified black body, which can be attributed to emission from hot dust. Figure 5 shows the NP spectrum of the filament together with a fitted modified black body of $T = 868$ K with the emissivity of $\propto \lambda^{-2}$. The modified black body curve closely reproduces the observed spectrum, suggesting a similarity to the excess continuum in normal galaxies and a hot dust origin for the excess emission. If the spiky features at 3.75 and 4.05 μm are assumed to be P γ and Br α , the associated free-free emission is expected. Simple estimates of the intensities of the two lines obtained by integrating over the continuum infer 2.8×10^{-9} and 2.4×10^{-9} W m⁻² sr⁻¹ for P γ and Br α , respectively. The line ratio differs significantly from the case A or B, which infers that there is a large uncertainty in the estimated line intensities. Far stronger P β than P γ emission should be present around 4.65 μm , where only a marginal hump is seen. The strength of the hump is compatible with the estimated Br α intensity. Thus we estimate the intensity of the free-free emission from the Br α intensity. For the case B with the electron temperature of 10^4 K, the free-free intensity expected from the Br α intensity is about 0.03 MJy sr⁻¹. Therefore, the free-free emission alone cannot account for the observed excess continuum emission and a hot dust contribution may be needed even considering the large uncertainty in the estimated line intensity.

5. Summary

We have presented *AKARI*/IRC observations of the starburst dwarf galaxy NGC1569. Imaging observations have detected the MIR UIR band emission in a H α filament, which is formed

by the outflow originating in the star-formation activities of the NGC1569 disk. Subsequent spectroscopic observations also with the IRC clearly confirm the presence of the UIR bands at 3.3, 6.2, 7.7, and 11.3 μm in the filament. A comparison with the IRS spectrum of the disk of NGC1569 suggests that the UIR bands in the filament have a lower ratio of the 7.7 to 11.3 μm band strength than in the galaxy disk. The low band ratio is also measured for the outflow or halo regions of other galaxies in addition to elliptical galaxies and the interarm regions of our Galaxy. Common characteristics may be attributed to the processing of the band carriers in these tenuous regions.

Thermal sputtering in the outflow is estimated to be very efficient and we propose that the band carriers cannot survive in the outflow. Alternatively, we suggest that the band carriers may be formed by the fragmentation of larger carbonaceous grains in the shock that produces the H α emission.

The presence of excess continuum emission in the NIR is also indicated by the present spectroscopy in addition to the 3.3 μm UIR band. The present spectrum implies both that the excess continuum emission cannot be accounted for solely by the free-free emission estimated from the Br α that is possibly detected and that hot dust emission may be an important contributor.

Acknowledgements. This work is based on observations with *AKARI*, a JAXA project with the participation of ESA. The authors thank all the members of the *AKARI* project and the members of the Interstellar and Nearby Galaxy team for their help and continuous encouragements. Part of this work is based on observations made with the *Spitzer Space Telescope*, which is operated by the Jet Propulsion Laboratory (JPL), California Institute of Technology under a contract with the National Aeronautics and Space Administration (NASA). This work has also made use of the NASA Extragalactic Database (NED) which is operated by the JPL, California Institute of Technology under contract with NASA. The authors thank T. L. Roellig and Y. Y. Tajiri for providing us with the IRS spectrum of NGC1569. They also thank S. Mühle for providing their H I data. This work is supported by a Grant-in-Aid for Scientific Research from the Japan Society for the Promotion of Science (no. 18204014).

References

- Allamandola, L. J., Tielens, A. G. G. M., & Barker, J. R. 1985, *ApJ*, 290, L25
 An, J. H. & Sellgren, K. 2003, *ApJ*, 599, 312
 Angeretti, L., Tosi, M., Greggio, L., Sabbi, E., Aloisi, A., & Leitherer, C. 2005, *AJ*, 129, 2203
 Buckalew, R. A., & Kobulnicky, A. 2006, *AJ*, 132, 1061
 Buckalew, R. A., Dufour, R. J., Shopbell, P., & Walter, D. K. 2000, *AJ*, 120, 2402
 Chan, K.-W., Roellig, T. L., Onaka, T., et al. 2001, *ApJ*, 546, 273
 Chernetoff, I., Baker, J. R., & Tielens, A. G. G. M. 1992, *ApJ*, 401, 269
 Cohen, M., Green, A. K., Meade, M. R., et al. 2007, *MNRAS*, 374, 979
 Draine, B. T., Dale, D. A., Bendo, G., et al. 2007, *ApJ*, 663, 866
 Engelbracht, C. W., Gordon, J. D., Rieke, G. H., Werner, M. W., Dale, D. A., & Latter, W. B. 2005, *ApJ*, 628, 29
 Engelbracht, C. W., Kundurthy, P., Gordon, K. D., et al. 2006, *ApJ*, 642, L127
 Engelbracht, C. W., Rieke, G. H., Gordon, K. D., et al. 2008, *ApJ*, 678, 804 (Erratum *ApJ*, 685, 678)
 Frenklach, M., & Feigelson, E. D. 1989, *ApJ*, 341, 372
 Flagey, N., Boulanger, F., Verstraete L., Miville Deschênes, M. A., Noriega Crespo, A., & Reach, W. T. 2006, *A&A*, 989
 Galliano, F., Dwek, E., & Chantial, P. 2008a, *ApJ*, 672, 214
 Galliano, F., Madden, S. C., Tielens, A. G. G. M., Peeters, E., & Jones, A. P. 2008b, *ApJ*, 679, 310
 Giard, M., Pajot, F., Lamarre, J. M., et al. 1988, *A&A*, 201, L1
 Gordon, K. D., Engelbracht, C. W., Rieke, G. H., et al. 2008, *ApJ*, 682, 336
 Greenberg, J. M., Gillett, J. S., Munõz Caro, G. M. et al. 2000, *ApJ*, 531, L71
 Greggio, L., Tosi, M., Clampin, M., et al. 1998, *ApJ*, 504, 725
 Greve, A., Tarchi, A., Hüttemeister, S., de Grijs, R., van der Hulst, J. M., Garrington, S. T., & Neinger, N. 2002, *A&A*, 381, 825
 Grocholski, A. J., Aloisi, A., Roeland, P., et al. 2008, *ApJ*, 686, L79
 Heckman, T. M., Dahlem, M., Lehnert, M. D., et al. 1995, *ApJ*, 448, 98
 Helou, G., Lu, N. Y., Werner, M. W., Malhotra, S., & Silberman, N. 2000, *ApJ*, 532, L21
 Herbst, E. 1991, *ApJ*, 366, 133
 Hodge, P. W. 1974, *ApJ*, 191, L21
 Hunter, D. A., Hawley, W. N., & Gallagher III, J. S. 1993, *AJ*, 106, 1797
 Hunter, D. A., O'Connell, R. W., Gallagher, J. S., & Smecker-Hane, T. A. 2000, *AJ*, 120, 2383
 Hunter, D. A., & Elmegreen, B. G. 2004, *AJ*, 128, 2170
 Hunter, D. A., van Woerden, H., & Gallagher, J. S. 2006, *AJ*, 132, 801
 Irwin, J. A., & Madden, S. 2006, *A&A*, 445, 123
 Irwin, J. A., Kennedy, H., Parkin, T., & Maddeen, S. 2007, *A&A*, 474, 461
 Ishihara, D., Onaka, T., Kaneda, H., et al. 2007, *PASJ*, 59, S443
 Jones, A. P., Tielens, A. G. G. M., & Hollenbach, D. J. 1996, *ApJ*, 469, 740
 Kahanpää, J., Mattila, K., Lehtinen, K., Leinert, C., & Lemke, D. 2003, *A&A*, 405, 999
 Kaneda, H., Onaka, T., & Sakon, I. 2005, *ApJ*, 632, L83
 Kaneda, H., Onaka, T., & Sakon, I. 2007, *ApJ*, 666, L21
 Kaneda, H., Onaka, T., Sakon, I., et al. 2008, *ApJ*, 684, 270
 Kaneda, H., Koo, B.-C., Onaka, T., & Takahashi, H. 2009a, *Adv. Sp. Res.*, 44, 1038
 Kaneda, H., Yamagishi, M., Suzuki, T., & Onaka, T. 2009b, *ApJ*, 698, L125
 Kaneda, H., Ishihara, D., Suzuki, T., et al. 2010, *A&A*, submitted
 Kelsall, T., Weiland, J. L., Franz, B. A., et al. 1998, *ApJ*, 508, 44
 Latter, W. B. 1991, *ApJ*, 377, 187
 Léger, A. & Puget, J. L. 1984, *A&A*, 137, L5
 Lu, N., Helou, G., Werner, M. W., et al. 2003, *ApJ*, 588, 199
 Lutz, D., Valiante, E., Sturm, E., et al. 2005, *ApJ*, 625, L83
 Madden, S., Galliano, F., Jones, A. P., & Sauvage, M. 2006, *A&A*, 446, 877
 Martin, C. L. 1998, *ApJ*, 506, 222
 Martin, C. L., Kobulnicky, H. A., & Heckman, T. M. 2002, *ApJ*, 574, 663
 Mattila, K., Lemke, D., Haikala, L. K., et al. 1996, *A&A*, 315, L353
 Matsumoto, H., Sakon, I., Onaka, T. et al. 2008, *ApJ*, 677, 1120
 Mühle, S., Klein, U., Wilcots, E. M., & Hüttemeister, S. 2005, *AJ*, 130, 524
 Murakami, H., Baba, H., Barthel, P., et al. 2007, *PASJ*, 59, S369
 O'Halloran, B., Satyapal, S., & Dudik, R. P. 2006, *ApJ*, 641, 795
 Ohyama, Y., Onaka, T., Matsuhara, H., et al. 2007, *PASJ*, 59, S411
 Omont, A. 1986, *A&A*, 164, 159
 Onaka, T. 2000, *Adv. Sp. Res.*, 25, 2167
 Onaka, T. 2004, in *Astrophysics of Dust*, eds. A. N. Witt, G. C. Clayton, and B. T. Draine, *ASP Conf. ser.* 309, 163
 Onaka, T., Yamamura, I., Tanabé, T., Roellig, T. L., & Yuen, L. 1996, *PASJ*, 48, L59
 Onaka, T., Tokura, D., Sakon, I., et al. 2007a, *ApJ*, 654, 844
 Onaka, T., Matsuhara, H., Wada, T., et al. 2007b, *PASJ*, 59, S401
 Onaka, T., Matsumoto, H., Sakon, I., & Kaneda, H. 2008, *Proc. of IAU Symp. No. 251, Organic Matter in Space*, eds. S. Kwok & S. Sandford, 229
 Ott, J., Walter, F., & Brinks, E. 2005, *MNRAS*, 358, 1453
 Pahre, M. A., Ashby, M. L. N., Fazio, G. G., & Willner, S. P. 2004, *ApJS*, 154, 229
 Papoular, R., Conard, J., Giuliano, M., Kister, J., & Mille, G. 1989, *A&A*, 217, 204
 Peeters, E., Hony, S., van Kerckhoven, C., et al. 2002, *A&A*, 390, 1089
 Peeters, E., Spoon, H. W. W., & Tielens, A. G. G. M. 2004, *ApJ*, 613, 986
 Reach, W. T., Megeath, S. T., Cohen, M., et al. *PASP*, 117, 978
 Sakata, A., Wada, S., Tanabé, T., & Onaka, T. 1984, *ApJ*, 287, L51
 Sakon, I., Onaka, T., Ishihara, D., et al. 2004, *ApJ*, 609, 203 (Erratum: *ApJ*, 625, 1062)
 Sakon, I., Onaka, T., Wada, T., et al. 2007, *PASJ*, 49, S483
 Sellgren, K., Werner, M. W., & Dinerstein, H. L. 1983, *ApJ*, 271, L13
 Sellgren, K. 1984, *ApJ*, 277, 623
 Smith, J. D., Draine, B. T., Dale, D. A., et al. 2007, *ApJ*, 656, 770
 Smith, B. J., Struck, C., Hancock, M., et al. 2007, *AJ*, 133, 791
 Smith, B. J. & Hancock, M. 2009, *AJ*, 138, 130
 Stil, J. M. & Israel, F. P. 1998, *A&A*, 337, 64
 Tacconi-Garman, L. E., Sturm, E., Lehnert, M., Lutz, D., Davies, R. I., & Moorwood, A. F. M. 2005, *A&A*, 432, 91
 Tajiri, Y. Y., Onaka, T., Okada, Y., Roellig, T. L., & Chan, K.-W. 2008, *ASP Conf. ser.* 381, 50
 Tanabé, T., Sakon, I., Cohen, M., et al. 2008, *PASJ*, 60, S375
 Tanaka, M., Matsumoto, T., Murakami, H., et al. 1996, *PASJ*, 48, L53
 Tielens, A. G. G. M. 2008, *ARA&A*, 46, 289
 Tielens, A. G. G. M., McKee, C. F., Seab, C. G., & Hollenbach, D. J. 1994, *ApJ*, 431, 321
 Tokura, D., Onaka, T., Takahashi, H., et al. 2007, *ApJ*, 648, 355
 van Kerckhoven, C., Hony, S., Peeters, E. et al. 2000, *A&A*, 357, 1013
 Wada, S., Onaka, T., Yamamura, I., Murata, Y., & Tokunaga, A. T. 2003, *A&A*, 407, 551
 Werner, M. W., Uchida, K. I., Sellgren, K., et al. 2004, *ApJS*, 154, 309
 Westmoquette, M. S., Exter, K. M., Smith, L. J., & Gallagher III, J. S. 2007a, *MNRAS*, 381, 894

- Westmoquette, M. S., Smith, L. J., Gallagher III, J. S., & Exter, K. M. 2007b, MNRAS, 381, 913
- Westmoquette, M. S., Smith, L. J., Gallagher III, J. S. 2008, MNRAS, 383, 864
- Wu, Y., Charmandaris, V., Hao, L., et al. 2006, ApJ, 639, 157
- Wu, H., Zhu, Y.-N., Cao, C., & Qin, B. 2007, ApJ, 668, 87